crystals

MDPI

Article

Optimization of the Mechanical and Corrosion Resistance of Alloy 625 through Aging Treatments

Barbara Rivolta, Riccardo Gerosa, Davide Panzeri * and Arsalan Nazim

Department of Mechanical Engineering, Politecnico di Milano, via La Masa 1, 20156 Milan, Italy; barbara.rivolta@polimi.it (B.R.); riccardo.gerosa@polimi.it (R.G.); arsalan.nazim@mail.polimi.it (A.N.)
* Correspondence: davide.panzeri@polimi.it

Abstract: In the as-annealed condition, the nickel-based Alloy 625 has excellent mechanical and corrosion properties compared to those of common stainless steels. This peculiarity enables its exploitation in several industrial fields at cryogenic and high temperatures and in the presence of severely corrosive atmospheres. However, in this alloy, when high-temperature plastic deformation processes and heat treatments are not carefully optimized, the occurrence of excessive grain coarsening can irremediably deteriorate the mechanical strength, possibly leading to incompatibility with the standard requirements. Therefore, this research work investigated the possibility of adopting single- and double-aging treatments aimed at improving such strength loss. Their optimization involved identifying the best compromise between the hardening effect and the loss in corrosion resistance induced by the simultaneous formation of intergranular chromium-rich carbides during aging. The investigation of the aging treatments was performed using hardness, tensile and intergranular corrosion tests considering different time–temperature combinations in a range from 621 °C to 732 °C. Double aging resulted in a considerable acceleration in the hardening response compared to single aging. However, even after its optimization in terms of both temperature and time, the intergranular corrosion resistance remained a critical aspect. Among all the tested conditions, only single aging at 621 °C for 72 h was acceptable in terms of both mechanical and corrosion properties. The influence of longer exposures will be investigated in a future study.

Keywords: superalloys; alloy 625; aging treatment; mechanical property; corrosion resistance

Citation: Rivolta, B.; Gerosa, R.; Panzeri, D.; Nazim, A. Optimization of the Mechanical and Corrosion Resistance of Alloy 625 through Aging Treatments. *Crystals* **2024**, *14*, 139. https://doi.org/10.3390/cryst14020139

Academic Editor: Pavel Lukáč

Received: 4 December 2023
Revised: 18 January 2024
Accepted: 26 January 2024
Published: 30 January 2024

1. Introduction

Alloy 625 is a nickel–chromium–molybdenum alloy patented in 1964. Owing to the presence of relatively high contents of Cr, Mo and Nb, this alloy provides an excellent combination of mechanical strength, weldability, corrosion resistance and fatigue properties [1–11]. The high mechanical strength and resistance of this material to several corrosive media allow its adoption in many fields, such as aerospace, oil and gas extraction, power generation and automotive applications, where superior mechanical properties are needed [1,4,6,11]. According to the ASTM B446 standard [12], this alloy is available in soft- and solution-annealed conditions, and it attains the optimal combination of mechanical properties and corrosion resistance compared to common stainless steels [4,6,13]. The minimum soft annealing temperature is 871 °C, and it is recommended for applications below 600 °C, where tensile strength and corrosion resistance are needed [12]. The minimum solution annealing temperature is 1093 °C, which is suggested for applications above 600 °C, where high creep strength is required [12].

After soft-annealing treatment, the microstructure is fully austenitic, and primary carbides and nitrides are normally heterogeneously dispersed in the matrix [8–11,14,15]. These compounds are formed during solidification and mainly include niobium and titanium, leading to the depletion of these alloying elements in the surrounding regions [9]. The thermal exposure during processing, heat treatment and service can determine the

precipitation of secondary phases. In fact, the presence of titanium, niobium, aluminum, chromium and molybdenum can activate complex precipitation phenomena with sufficient exposure above approximately 600 °C [9,10,15,16]. The formation of precipitates can strongly modify the mechanical properties and corrosion resistance with respect to the as-annealed condition [1,9]. The time–temperature–precipitation (TTP) curves available in the literature are reported and adapted in Figure 1 [9]. In particular, according to this diagram, the precipitate phases can be MC, M_6C and $M_{23}C_6$ metal carbides, intermetallic phases, normally γ'', δ, Ni_2(Cr,Mo) and Laves, and $(Cr,Nb)_2N$ nitrides [9,15,17]. The chemical compositions of the primary and secondary phases are given in Table 1. The precipitation curve of the Ni_2(Cr,Mo) phase with snowflake morphology is not shown in Figure 1. In fact, according to the literature, it is formed after very long exposures below 600 °C, and these time–temperature aging conditions lie outside the ranges investigated in this research. Its precipitation kinetics have not been investigated in depth in the literature [18,19]. The formation of intergranular carbides and intermetallic phases determines sensitization and the reduction in ductility and deformability [4,20,21]. In fact, intergranular chromium- and molybdenum-rich carbides deplete such alloying elements from their surroundings, resulting in a local reduction in the resistance to intergranular corrosion [1–4,9,15,20–22]. Moreover, the formation of intergranular carbide films promotes intergranular cracking with a consequent decrease in toughness. For this reason, during service and cooling from the annealing temperature, exposure above 600 °C should be carefully monitored to avoid the formation of precipitate phases. However, the controlled formation of intermetallic phases can be exploited to obtain a hardening effect [15,19].

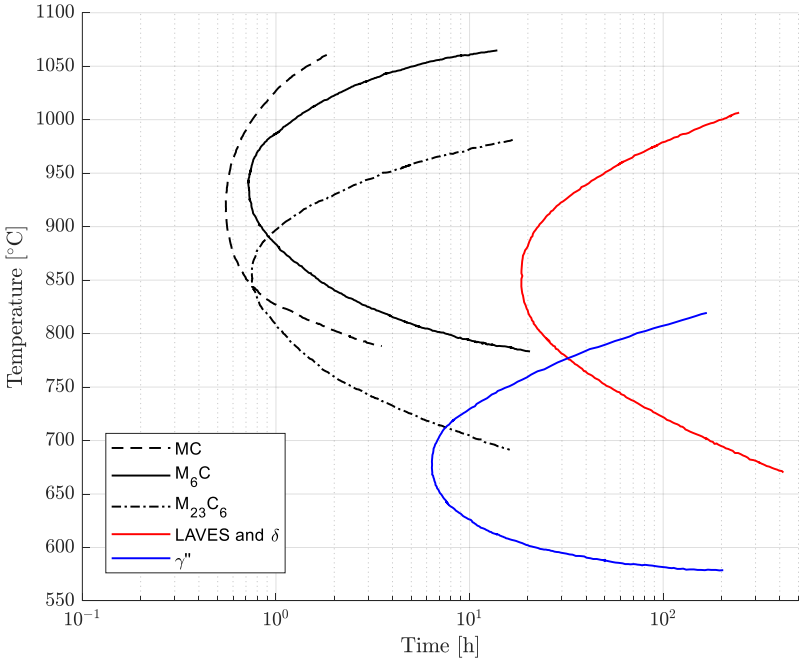

Figure 1. Time–temperature–precipitation (TTP) curves of Alloy 625. Composition ranges in wt. %: 0.01–0.04 C, 0.05–0.10 Si, 0.02–0.10 Mn, 20.5–22.5 Cr, 4.0–4.5 Fe, 8.1–8.9 Mo, 0.1–0.25 Ti, 3.4–3.7 Nb, 0.02–0.03 Al [9].

Table 1. Chemical compositions of the primary and secondary phases typically observed in Alloy 625. Adapted from [1,9].

Phase	Typical Composition
MC	Matrix blocky
	$(Cr_{0.04}Fe_{0.02}Ni_{0.09}Nb_{0.75}Mo_{0.03}Ti_{0.07})C$
	$(Cr_{0.03}Ni_{0.04}Nb_{0.39}Mo_{0.01}Ti_{0.53})C$
	Grain boundary
	$(Cr_{0.04}Fe_{0.01}Ni_{0.08}Nb_{0.67}Mo_{0.01}Ti_{0.15})C$
M_6C	$(Cr_{0.21}Fe_{0.02}Ni_{0.37}Nb_{0.80}Mo_{0.24}Si_{0.08})_6C$
$M_{23}C_6$	$(Cr_{0.85}Fe_{0.01}Ni_{0.07}Mo_{0.07})_{23}C_6$
γ''	$Ni_3(Nb_{>0.5}Ti_{<0.5}Al_{<0.5})$
δ	Ni_3Nb
$Ni_2(Cr,Mo)$	$Ni_{0.63}Cr_{0.30}Mo_{0.07}$
Laves	$(Cr_{0.31}Fe_{0.08}Ni_{0.41})_2(Si_{0.17}Ti_{0.01}Nb_{0.19}Mo_{0.63})$
$(Cr,Nb)_2N$	$(Cr_{0.39}Nb_{0.41}Ni_{0.07}Mo_{0.13})_2N$

In nickel-based superalloys, grain refinement can occur only during high-temperature plastic deformation if the thermomechanical conditions are well studied and controlled. During solution- and soft-annealing treatments, which are performed at high temperatures, the grain size can increase very quickly depending on the treatment time and temperature. For such a reason, it is difficult to obtain a fine-grained structure and, very often, the average size is significantly larger than that achievable for a component with the same geometry but made of steel. Consequently, the temperature range of the annealing treatment inevitably determines grain growth [11,23,24], and its severity strongly depends on the temperature and soaking time. Since the mechanical properties are strongly affected by grain size, heat treatment parameters should be determined based on the best compromise between solubilization efficacy, which affects corrosion resistance, and grain growth, which directly influences mechanical strength. The influence of annealing temperature and soaking time on grain size and mechanical properties was studied in the literature by Rivolta et al. [11]. The possibility of increasing the mechanical resistance by means of an aging treatment at medium-to-low temperatures is, hence, particularly interesting. Such an improvement is generally associated with a deformability reduction that should be considered in the tuning of aging parameters.

As described, the incompatibility of the tensile properties of this alloy with the standard requirements is a common industrial issue [12]. In fact, the ability to retain a fine grain size after processing and heat treatment is critical. According to the processing map of this material and its flow stress behavior [25–27], the region associated with complete recrystallization is very narrow, and strict equipment requirements are imposed. Therefore, considering such peculiarities, an accurate design of the plastic deformation process becomes mandatory. However, depending on the component geometry and the available equipment, the deformation process is often performed outside the optimal working region, possibly leading to excessive grain coarsening. This detrimental phenomenon is further worsened by subsequent annealing treatments. In nickel-based superalloys, the possibility of retaining a fine grain size after high-temperature processing and heat treatment is a critical aspect. Moreover, the absence of phase transformation temperatures prevents the possibility of refining grains through heat treatment. According to the Hall–Petch relation and as reported by Rivolta et al. [11], an increase in grain size determines a decrease in mechanical performance. In this case, the mechanical strength can become incompatible with the standard requirements [12]. The unique possibility of recovering such property loss is represented by age-hardening treatments. In fact, even though Alloy 625 was developed

as a solid solution-strengthened alloy, the presence of sufficient amounts of niobium, titanium and aluminum allows for precipitation of the intermetallic hardening γ'' phase upon thermal exposure in a range from 600 °C to 800 °C [9,16,17]. However, in this temperature range, the simultaneous formation of intergranular Cr-rich carbides detrimental to corrosion resistance can occur, especially after short exposures above 700 °C. The ASTM B446 standard does not prescribe any kind of aging treatment [12]. In the literature, the single-aging response was studied using hardness tests in a range from 600 °C to 800 °C by Moore et al. [24] and from 550 °C to 900 °C by Suave et al. [1,19], which resulted in an appreciable increase in hardness only after very long exposures. Consequently, considering that the occurrence of a very slow precipitation response upon single aging can limit its industrial exploitation, this research work aimed to investigate the possibility of faster age-hardening procedures based on tailored nonstandard double-aging treatments while maintaining corrosion resistance within acceptable limits. For this reason, a preliminary analysis of the influence of single-aging treatments on the mechanical and corrosion properties was performed. These results provide the basis for the definition of the experimental plan for double-aging treatments and their investigation. Therefore, tailored aging treatments can be developed and optimized to provide a strength enhancement sufficient to comply with the standard requirements. The optimization of the tensile properties can also be exploited to reduce the thickness and mass, with a consequent decrease in the consumption of resources and carbon footprint. Currently, the sustainability of a process and of a product is of primary importance. A reduction in the carbon footprint and consumption of resources can be achieved through careful control of all the manufacturing stages. Enhancements in the material mechanical performance were traditionally associated with the possibility of decreasing the component weight, resulting in a reduction in costs and fuel consumption. Nevertheless, the possibility of enabling material savings also limits the environmental impact associated with raw material extraction and processing. This consideration is particularly important for high-energy-demanding processes, such as nickel-based superalloy production.

The precipitation-hardening response is studied considering different time–temperature combinations upon single and double aging. The temperatures were selected starting from the aging procedure currently adopted for the alloy CarTech® Custom Age 625 PLUS® [28,29]. This grade is a variant of the conventional Alloy 625, and the unique difference is the titanium content, which is 1 wt. % higher. This compositional variation promoted the formation of γ'' Ni_3Nb precipitates [17,28]. In this case, the double-aging treatment is adopted to accelerate the age-hardening response compared to single-aging treatments. For this variant, according to the standard procedure [28,29], after soft-annealing treatment at 1038 °C, primary aging is performed at 732 °C for 8 h, followed by furnace cooling and secondary aging at 621 °C 8 h. Therefore, considering these two temperature levels as the starting point for this research work, this aging procedure was also investigated in Alloy 625. In this case, different time–temperature combinations for single and double aging were studied using hardness, tensile and corrosion tests. To evaluate the corrosion behavior, tests were performed according to the standard ASTM G28-A [30]. This standard is related to the investigation of the susceptibility to intergranular corrosion in a solution of ferric sulfate, $Fe_2(SO_4)_3$ and sulfuric acid, H_2SO_4, for 120 h [30].

According to the available online literature about the influence of double-aging treatments on the mechanical and corrosion properties, only a few results were found. For instance, Eiselstein and Tillack [7] reported that sufficient soaking in a temperature range from 732 °C to 843 °C is required to trigger the precipitation reaction and permit faster aging at 649 °C. The authors investigated the aging response from 621 °C to 704 °C of Alloy 625 solution annealed at 1149 °C for 1 h and nucleation treated at 760 °C for 1 h. They confirmed the marked acceleration of the age-hardening kinetics with this multistage treatment [7]. However, considering that the temperature range suggested by Eiselstein and Tillack for nucleation treatment is critical for corrosion resistance because of the rapid simultaneous formation of intergranular carbides, this research also investigated the influ-

ence of lower primary aging temperatures on the balance between the mechanical strength and corrosion resistance. In fact, no information is present in the literature about such optimization of both the mechanical and corrosion properties. Consequently, because this balance is particularly critical, we reduced the primary aging temperature to lower values (710 °C, 680 °C and 650 °C) to limit the precipitation of intergranular chromium-rich carbides as much as possible. The corrosion tests were performed on a selection of the single- and double-aging conditions investigated in this work. Considering the common prescription for industrial application of this alloy, the limit for the corrosion rate was set equal to 1.20 mm/year.

In addition, to better analyze the precipitation response associated with the double-aging procedure, we suggested a model for the double-aging treatment based on the Larson–Miller parameter, which combines the effects of temperature and duration of primary aging.

2. Materials and Methods

All the samples for metallographic observations, hardness, tensile and intergranular corrosion tests were taken from a forged and untreated 60 mm diameter rod. All the heat treatments were performed in a laboratory furnace (Model Carbolite CWF 13/13). Tensile and corrosion specimens were obtained from the longitudinal direction of the rod. Samples for microstructural analyses and hardness tests were cut using silicon carbide cutoff wheels with a Remet (Model TR100 EV; sourced from Remet s.a.s., Bologna, Italy) cutting machine. Mounting was performed in hot thermosetting phenolic resin using a Metkon (Model Ecopress 50; sourced from Microcontrol N.T. Srl, Milano, Italy) mounting machine. Grinding and polishing were carried out using a Struers (Model Pedemax 2 + Planopol 3; sourced from Struers s.a.s., Arese, Italy) machine up to the mirror-polished condition. After grinding and polishing, chemical etching was performed in five parts HCl diluted in one part 30% H_2O_2 for approximately 10 s [5,31,32]. A Leica (Model DMR; sourced from Leica Microsystems S.r.l., Buccinasco, Italy) light optical microscope and a Zeiss (Model SIGMA 500; sourced from Carl Zeiss S.p.A., Milano, Italy) scanning electron microscope were used for the metallographic analyses. The determination of the average grain size in the soft-annealed condition was performed in accordance with the ASTM E112 standard [33]. In this case, the Heyn lineal intercept procedure was adopted using twelve linear intercept lines. The hardness was measured in HV30 Vickers scale using a Wolpert Testor 930 hardness tester according to the EN ISO 6507 standard [34]. In each condition, five hardness measurements were performed. The room-temperature tensile properties were investigated by tensile tests performed according to the EN ISO 6892 standard using round proportional specimens with an INSTRON model 4507 testing machine [35]. The susceptibility to intergranular corrosion was analyzed using a solution of ferric sulfate, $Fe_2(SO_4)_3$ and sulfuric acid, H_2SO_4, for 120 h according to the ASTM G28—Method A standard [30]. The reference standard considered in this work for the mechanical strength requirements of this alloy is the ASTM B446 standard [12]. Considering the maximum corrosion rate, a value of 1.20 mm/year was considered to be a common prescription for industrial applications of this grade. SEM and EDXS analyses were performed on a selection of metallographic samples. Qualitative EDXS analyses of the chemical composition were carried out using an OXFORD Altee Energy—Advanced detector available in the adopted SEM.

The chemical composition of the material adopted in this research is reported in Table 2. It is compatible with the compositional limits defined by the ASTM B446 standard [12]. The chemical composition of the as-received material was analyzed via optical emission spectroscopy using a Jobin Yvon OES spectrometer.

Table 2. Chemical composition in wt. % determined by OES spectroscopy of the forged rod adopted in this research work.

	Ni	Cr	Mo	Nb	Fe	Mn	Ti	Al	C	Si	P	S
wt. %	63.2	20.1	8.32	3.51	4.32	0.07	0.28	0.22	0.03	0.14	<0.01	<0.01

The samples for hardness tests and microstructural analyses were characterized by dimensions of 10 mm × 10 mm × 10 mm. The tensile specimens were machined from 12 mm diameter rods obtained from a 60 mm diameter rod using EDM. The specimens for corrosion tests were 25 mm × 25 mm × 7 mm. Before aging, all the metallographic samples and the tensile and corrosion specimens were subjected to soft-annealing treatment at 1038 °C for 0.5 h. Single-aging treatments were performed at 621 °C, 650 °C, 680 °C, 710 °C and 732 °C for up to 72 h of exposure. Double-aging treatments were performed varying the primary aging temperature from 732 °C to 650 °C and fixing the secondary aging temperature at 621 °C. After each heat treatment, all the samples and specimens were water quenched. Each experimental aging condition was subjected to a preliminary analysis via hardness tests. Then, according to the results, tensile and corrosion tests were performed in selected conditions. SEM and EDXS analyses were carried out to better investigate the results of the corrosion tests.

3. Results and Discussion

3.1. Soft-Annealed Condition

The conventional material was supplied in the as-forged condition. Soft-annealing treatment at 1038 °C for 0.5 h was performed using a laboratory furnace on all the hardness and metallographic samples and the tensile and corrosion specimens. The microstructure in the soft-annealed condition was investigated by metallographic analysis via light-optical and scanning electron microscopy. Figure 2 shows the presence of a fully austenitic microstructure with equiaxed and twinned grains, with an average size of 65 µm and the absence of intergranular carbides. The grain size distribution in the soft-annealed condition is shown in Figure 3.

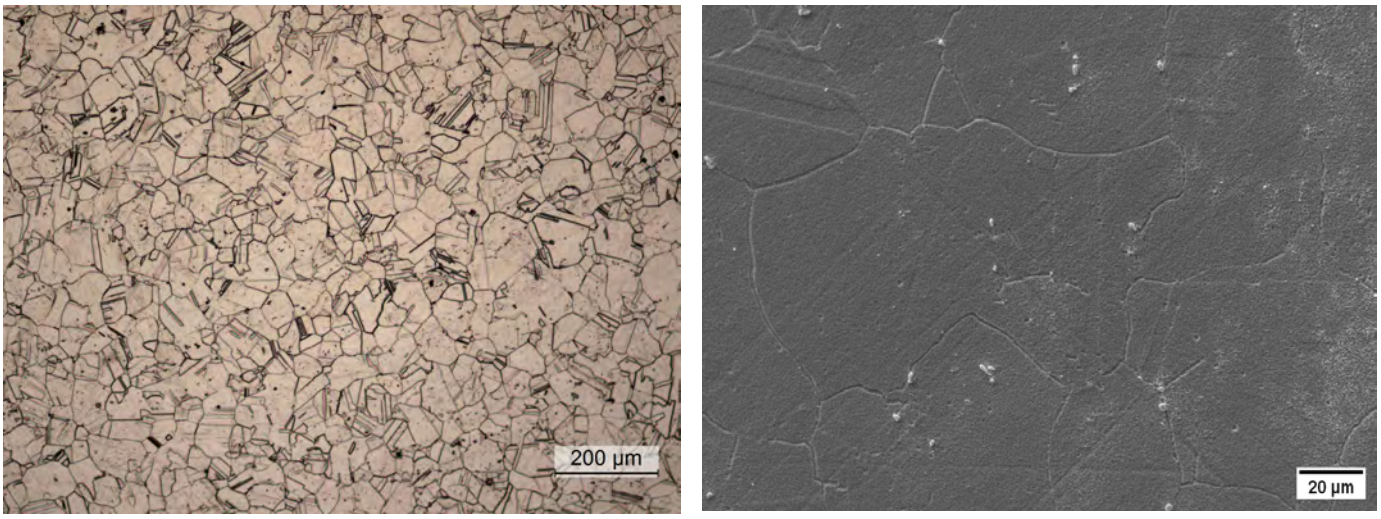

(**a**) (**b**)

Figure 2. Metallographic analysis of the soft-annealed material. (**a**) Light-optical micrograph; (**b**) scanning electron micrograph.

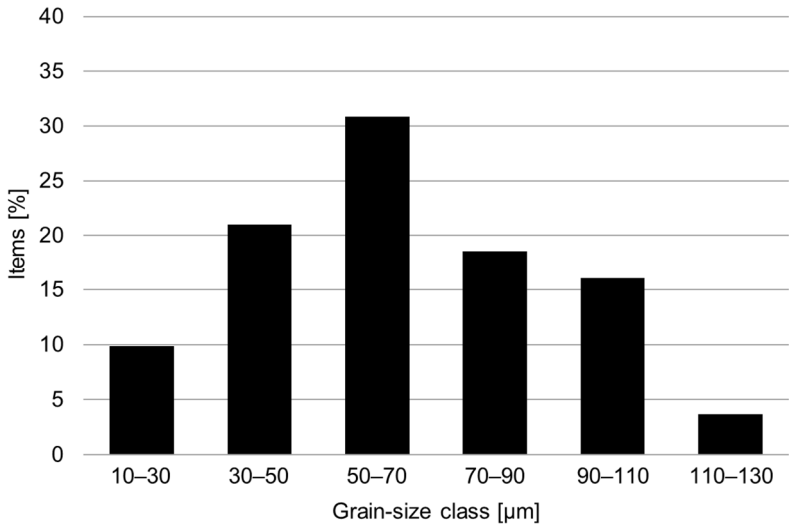

Figure 3. Grain size distribution in the soft-annealed condition (1038 °C for 0.5 h).

Then, the room-temperature mechanical properties of the conventional material in the soft-annealed condition were determined by tensile tests. The hardness, yield strength, ultimate tensile strength, percentage elongation after fracture A% and percentage reduction of area Z% are reported in Table 3. In the soft-annealed condition, the minimum yield strength prescribed by the ASTM B446 standard is 414 MPa [12]. Therefore, the mechanical strength does not comply with the minimum standard requirement. This issue is determined by the difficulties in maintaining a fine grain size during forging and heat treatment. The relation between the average grain size and the mechanical properties is compatible with the results reported in the literature by Rivolta et al. [11].

Table 3. Room-temperature mechanical properties compared to the minimum requirements defined by the ASTM B446 standard [12].

	Hardness	YS [MPa]	UTS [MPa]	YS/UTS	A%	Z%
This work	194 HV30	350	829	0.42	61.0	70
ASTM B446	---	>414	>827	---	>30.0	---

The susceptibility to intergranular corrosion was subsequently measured according to the ASTM G28 Method A standard [30]. After the 120 h corrosion test, the corrosion rate was 0.65 mm/year. This result confirmed the efficacy of the soft-annealing treatment at 1038 °C in retaining an acceptable corrosion resistance.

3.2. Single- and Double-Aging Treatments

The age-hardening response of the soft-annealed material (1038 °C 0.5 h) was investigated from 621 °C to 732 °C with isothermal single-aging treatments up to 72 h. The experimental single-aging curves are shown in Figure 4. According to the results, all the single-aging treatments provided only a slight increase in hardness. Most likely, the single-aging hardening response becomes significant only after excessively long exposures for most industrial applications. In the literature, the single-aging response of Alloy 625 was studied using hardness tests in a range from 600 °C to 800 °C by Moore et al. [24] and from 550 °C to 900 °C by Suave et al. [1,19], which resulted in an appreciable increase in hardness only after very long exposures. The hardness curves after single-aging treatment obtained in our research are in good agreement with the results reported by Moore et al. [24], confirming the occurrence of a very slow precipitation response when single aging is adopted. The increase in hardness upon single-aging treatment in a temperature range from 621 °C to 732 °C is determined by the formation of γ'' precipitates, as shown by

the time–temperature–precipitation diagram in Figure 1. According to these curves, the simultaneous formation of intergranular $M_{23}C_6$ carbides can occur, but their hardening effect is negligible compared to that provided by the intermetallic hardening γ'' phase [15].

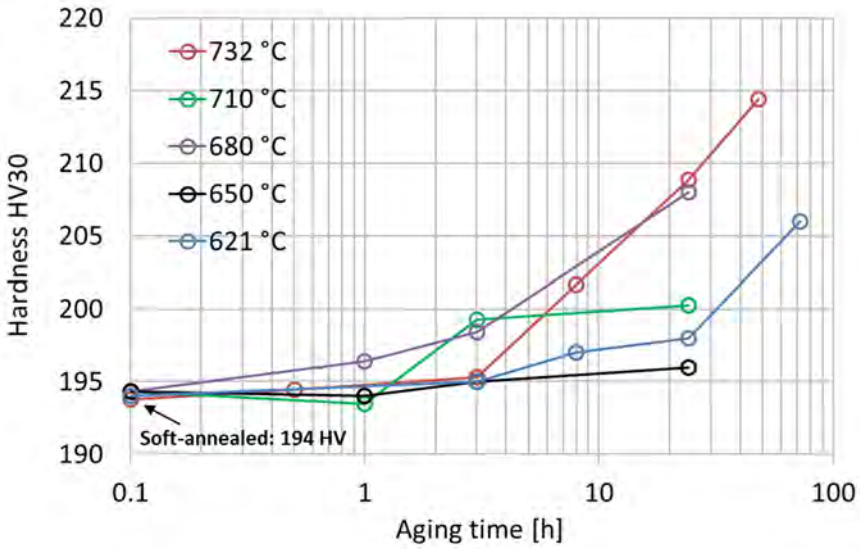

Figure 4. Vickers hardness HV30 experimental curves after isothermal single-aging treatments from 621 °C to 732 °C of the soft-annealed material. The standard deviations of these hardness measurements range from 1 HV30 to 3 HV30.

Double-aging treatments were performed considering a primary aging temperature varying from 732 °C to 650 °C and a fixed secondary aging temperature of 621 °C. As reported in Figure 5, the double-aging treatments resulted in a significant improvement in the age-hardening response compared to that associated with each single-aging treatment taken separately. For a fixed duration of the secondary aging at 621 °C, the precipitation-hardening effect is strongly enhanced with the addition of primary aging. However, excessively long primary aging times do not provide any appreciable further acceleration in the age-hardening response. For instance, considering primary aging at 732 °C, the hardness curves for primary exposures of 3 h, 16 h and 48 h almost overlap, as shown in Figure 5a. However, when the primary aging temperature is reduced, such behavior becomes less evident, and the double-aging hardness curves are closer to the single-aging curve because of the occurrence of a weaker acceleration. With respect to the double-aging treatment, Eiselstein and Tillack [7] reported a hardness increase from 52 HRA (166 HV) to 58 HRA (213 HV) for the solution-annealed Alloy 625 after nucleation treatment at 760 °C for 1 h and aging at 621 °C for 72 h. According to our experimental results, the hardness of 194 HV in the soft-annealed condition increases to 282 HV after double aging at 732 °C for 1 h and 621 °C for 72 h. After primary aging at 710 °C for 1 h, the hardness increased to 266 HV. After reducing the primary aging from 680 °C for 1 h to 650 °C for 1 h, the hardness was 225 HV and 215 HV, respectively. With respect to the alloy CarTech® Custom Age 625 PLUS®, as reported in the literature [28,29], the hardness in the soft-annealed condition was increased from 90 HRB (188 HV) to 37 HRC (353 HV) with the conventional double-aging procedure (732 °C for 8 h and 621 °C for 8 h). According to our experimental data, the same heat treatment conditions for Alloy 625 resulted in a hardness increase from 194 HV to 220 HV. This difference is mainly attributed to the lower titanium content of Alloy 625, which weakens and slows down its age-hardening response [28,29].

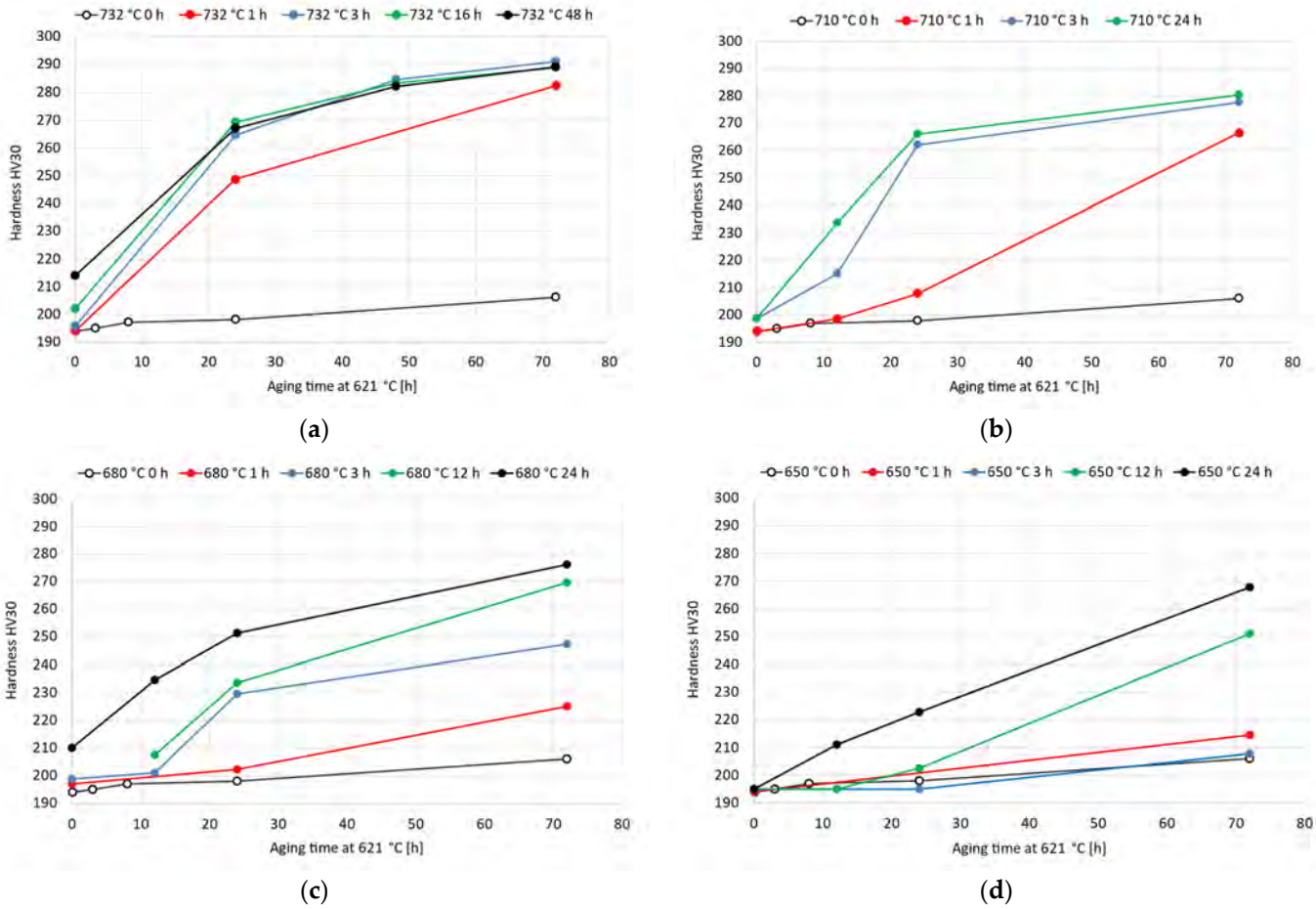

Figure 5. Vickers hardness HV30 experimental curves after double-aging treatments of the soft-annealed material varying the primary-aging temperature from 732 °C to 650 °C and with secondary aging temperature fixed at 621 °C: (**a**) 732 °C; (**b**) 710 °C; (**c**) 680 °C; (**d**) 650 °C. The standard deviations of these hardness measurements range from 1 HV30 to 6 HV30.

The grain size strongly influences the mechanical properties because the grain boundaries act as obstacles to dislocation movement. The grain-coarsening process is activated above a threshold temperature, which is equal to approximately 940 °C for this alloy grade [11]. Therefore, grain growth was not observed in the temperature ranges of both the single- and double-aging treatments investigated in this work. Regarding the formation of phases, as reported in the time–temperature–precipitation diagram in Figure 1, the precipitate particles generated upon single-aging treatments are intergranular Cr-rich $M_{23}C_6$ carbides and the intermetallic γ'' phase. The double-aging procedure allows γ'' precipitation to be accelerated due to the primary aging treatment, which promotes nucleation and the growth of subcritical γ'' nuclei [7,16]. This triggering effect is necessary to reduce the overall heat treatment time, which would be significantly longer in the case of single aging at 621 °C without prior nucleation treatment [7,16]. During the primary aging treatment, depending on the temperature, intermetallic $M_{23}C_6$ carbides can be formed according to the TTP curves reported in Figure 1 [7,15].

To better investigate the hardness increase induced by the double-aging treatment, the hardness process fraction curves were determined according to Equation (1) for each tested duration of the secondary aging at 621 °C. In particular, HV_0 is the double-aging hardness in the absence of primary aging. Therefore, this value coincides with the experimental hardness of single aging at 621 °C for the considered duration. HV_∞ represents the steady-state hardness value upon double aging for each considered secondary aging time. Their values are summarized in Table 4 and Figure 6. The experimental process fractions for each

secondary aging time are reported as a function of the Larson–Miller parameter (LMP_1) of the primary aging treatment in Figure 7. The expression of the LMP_1 parameter is given in Equation (2), where T_1 is the primary aging absolute temperature, C is a constant (set equal to 22) and t_1 is the primary aging time in hours. The adoption of the Larson–Miller parameter allows us to combine the effects of both the primary aging temperature and time into a single value. In general, creep, tempering of a quenched steel and precipitation of strengthening phases are typical phenomena that can be studied with this approach. The use of a single variable, the Larson–Miller parameter, simplifies the analysis of all the properties that change with respect to treatment temperature and time. This approach also allows for an easier correlation among these properties and the process parameters.

$$X_{HV}(LMP_1) = \frac{HV(LMP_1) - HV_0}{HV_\infty - HV_0} \quad (1)$$

$$LMP_1 = T_1(C + log_{10}t_1) \quad (2)$$

Table 4. Fitting parameters of the process–fraction curves based on the Avrami-type equation as a function of the duration of the secondary aging treatment (Time_2) in hours.

$Time_2$ [h]	HV_0	HV_∞	a	b
12	197	234	3.6×10^{-29}	8.5
24	198	267	7.7×10^{-17}	4.9
48	205	284	3.8×10^{-10}	2.9
72	206	290	1.0×10^{-8}	2.5

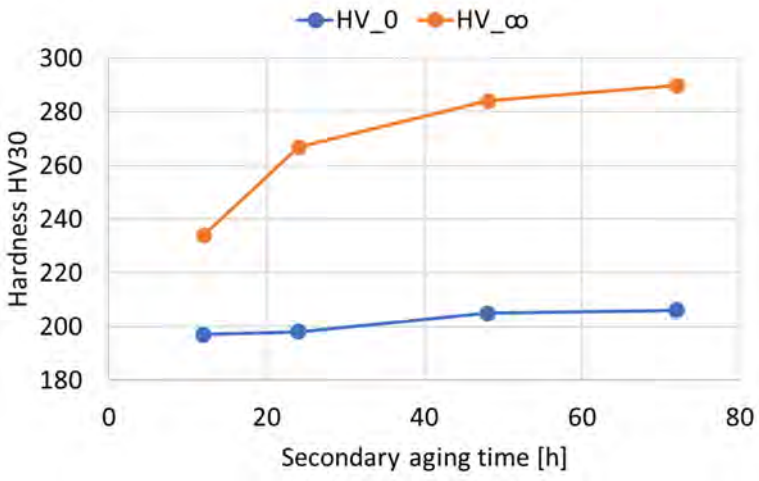

Figure 6. HV_0 and HV_∞ values as a function of the duration of the secondary aging treatment (Time_2) in hours.

The evolution of a process that involves a nucleation stage, a development and a transformation end can often be described by a sigmoidal curve, whose mathematical expression is given by the Avrami-type equation. In the metallurgical field, several structural transformations occur following these three stages, and, hence, they can be described using such a mathematical model. For this reason, the experimental process fractions were modeled using the Avrami-type equation with fitting parameters a and b, as reported in Equation (3), where LMP_1 is the Larson–Miller parameter of the primary aging treatment and LMP_0 is a constant set equal to 20,000 adopted to shift the "zero" of the process–fraction curves.

$$X_{HV}(LMP_1) = 1 - e^{-a(LMP_1 - LMP_0)^b} \quad (3)$$

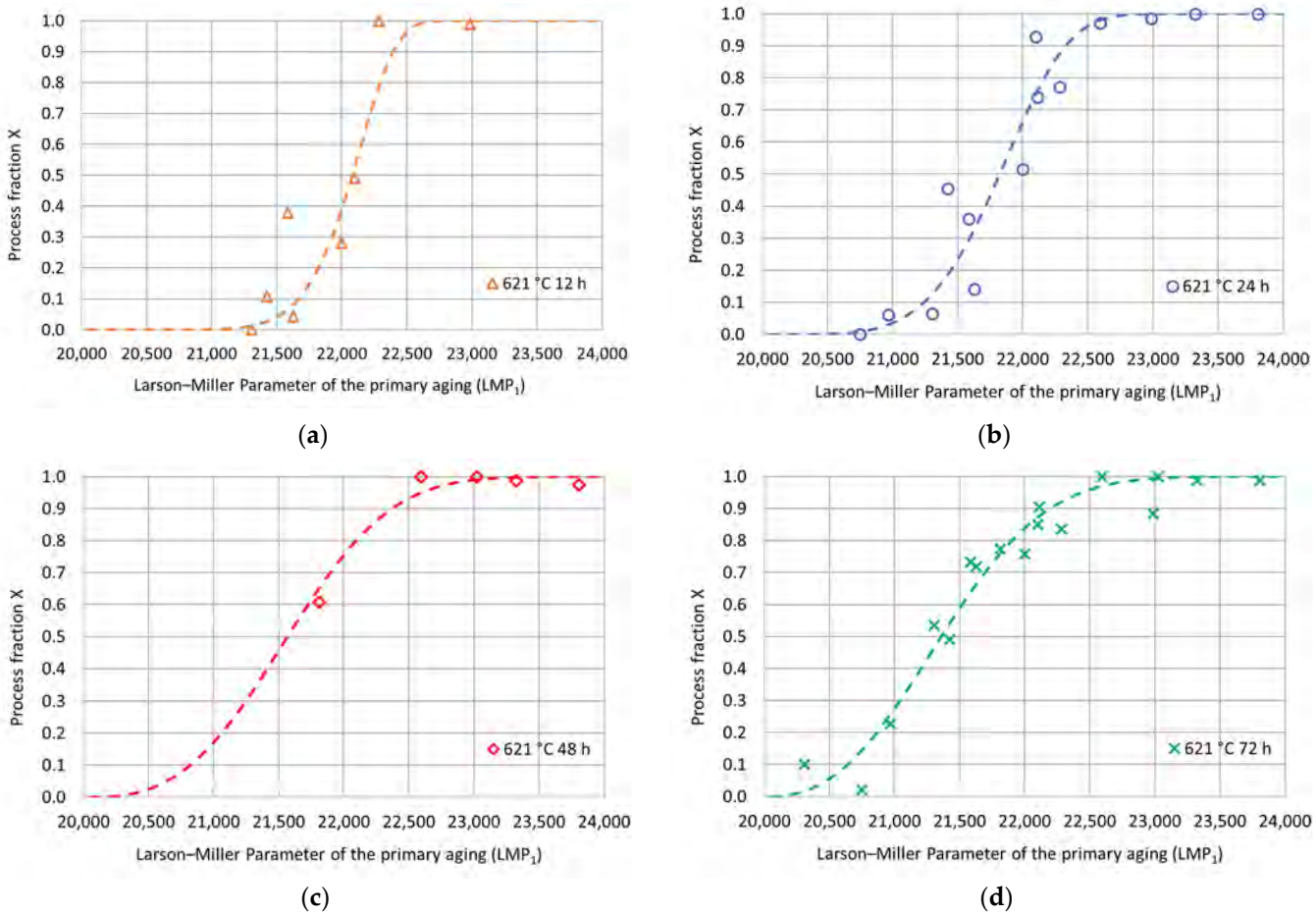

Figure 7. Experimental hardness process fractions and fitting curves as a function of the Larson–Miller parameter for the primary aging treatment for each secondary aging duration: (**a**) 621 °C 12 h; (**b**) 621 °C 24 h; (**c**) 621 °C 48 h; (**d**) 621 °C 72 h.

The fitting parameters *a* and *b* were determined using the least-square procedure, and the related values are reported in Table 4. The goodness of fit was assessed by calculating a determination coefficient equal to 0.97. The fitting curves are shown in Figure 7 as a function of the Larson–Miller parameter of the primary aging treatment. Then, for each secondary aging time, the experimental double-aging hardness values were represented as a function of the Larson–Miller parameter of the primary aging treatment together with the related fitting curves previously determined based on the process fractions. As shown in Figure 8, the comparison between the fitting curves and the experimental values together with the percentage error distribution confirm the goodness of fit of the adopted model.

The mathematical model of the double-aging hardness curves based on the Larson–Miller parameter yields very low percentage errors. Nevertheless, both the analyses could be improved by increasing the database width. For this reason, the authors have already planned new aging treatments to increase the number of experimental conditions and improve the accuracy of the model further.

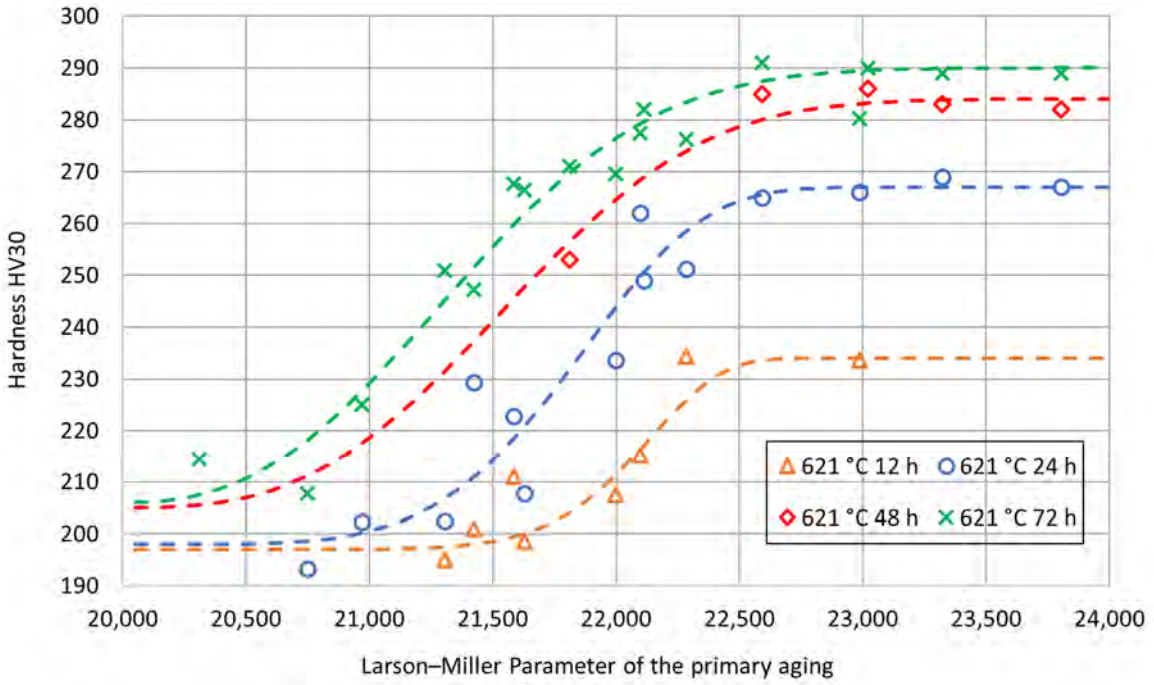

(**a**)

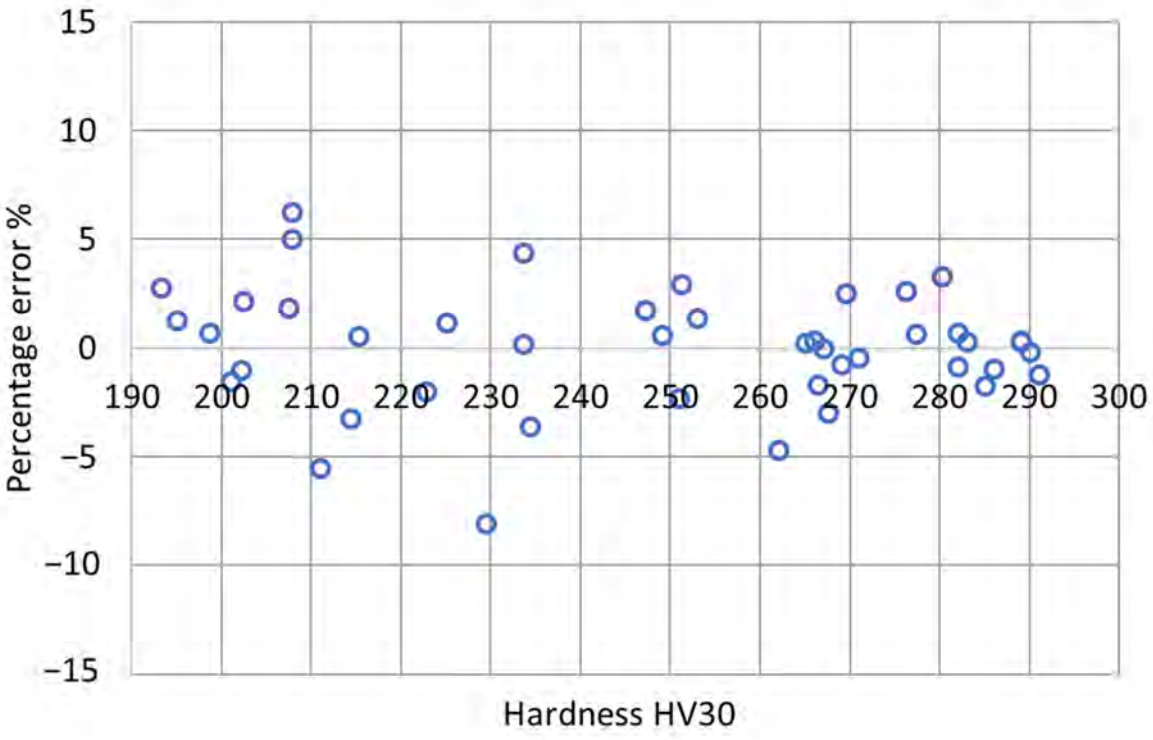

(**b**)

Figure 8. Experimental hardness values and fitting curves for each secondary aging time as a function of the Larson–Miller parameter of the primary aging treatment (**a**) and distribution of the percentage errors as a function of the hardness (**b**).

The room-temperature tensile properties were measured in selected conditions of the double-aging treatments at 732 °C and 621 °C to evaluate the influence of increasing aging time at both temperatures. As shown by the experimental results reported in Figure 9,

an increase in the duration of the secondary aging treatment at 621 °C improved the mechanical strength under fixed primary aging conditions. On the other hand, primary aging exposures longer than 3 h at 732 °C do not provide an appreciable increase in the tensile strength with fixed secondary aging. Therefore, after a certain duration of primary aging, the effect of acceleration on the age-hardening response is almost saturated. The strengthening effect induced by the precipitation of intermetallic phases is obtained at the expense of a reduction in the deformability, as shown by the values of A% and Z% in Figure 9. However, the deformability remains reasonable and well above the minimum standard requirement of 30% regarding the A% [12]. The tensile strength complied with the minimum standard requirements under all tested conditions [12]. This confirms the efficacy of properly designed aging treatments in improving insufficient mechanical properties induced by an excessive grain growth in the as-annealed condition.

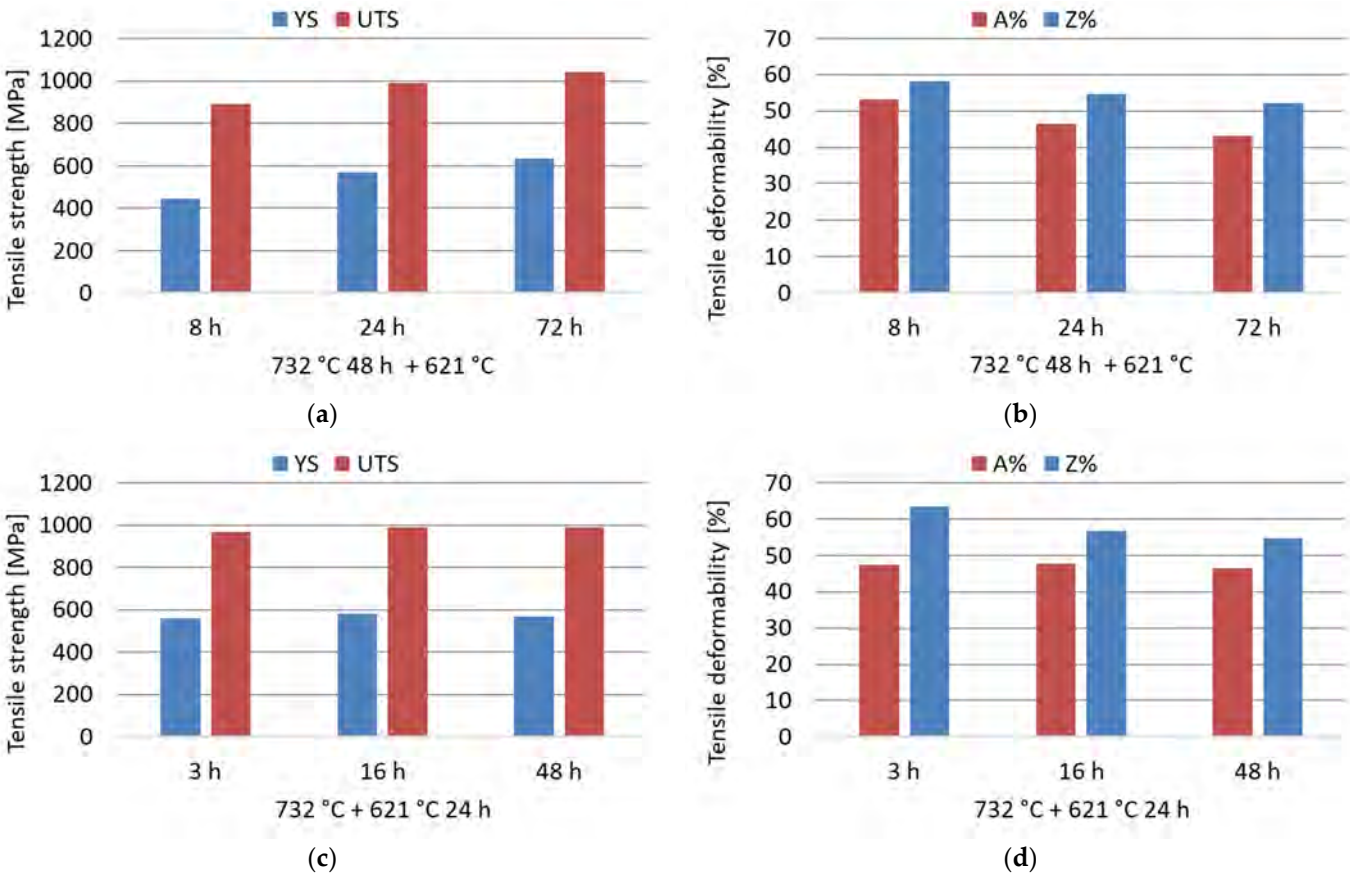

Figure 9. Room-temperature tensile properties (yield strength, YS; ultimate tensile strength, UTS; percentage elongation after fracture, A%; percentage reduction of area, Z%) of the soft-annealed material subjected to double-aging treatments at 732 °C and 621 °C for different times. (**a**,**b**) Influence of the increase in the secondary aging time; (**c**,**d**) influence of the increase in the primary aging time.

The relationship between the tensile strength (yield strength and ultimate tensile strength) and the hardness was determined by linear regression of the experimental results obtained in this work and those available in the literature [11]. The results of this analysis are reported in Figure 10. In this case, the goodness of fit of the linear regression model was assessed using the determination coefficient R^2. According to the linear regression parameters determined in this analysis and considering the minimum standard requirements for tensile strength [12], the minimum hardness value corresponding to the yield strength requirement is equal to 201 HV, and 192 HV for the ultimate tensile strength. Therefore, to satisfy both prescriptions, a minimum hardness of 201 HV is needed. This information

is extremely useful for performing a preliminary identification of the aging conditions potentially acceptable in terms of mechanical strength.

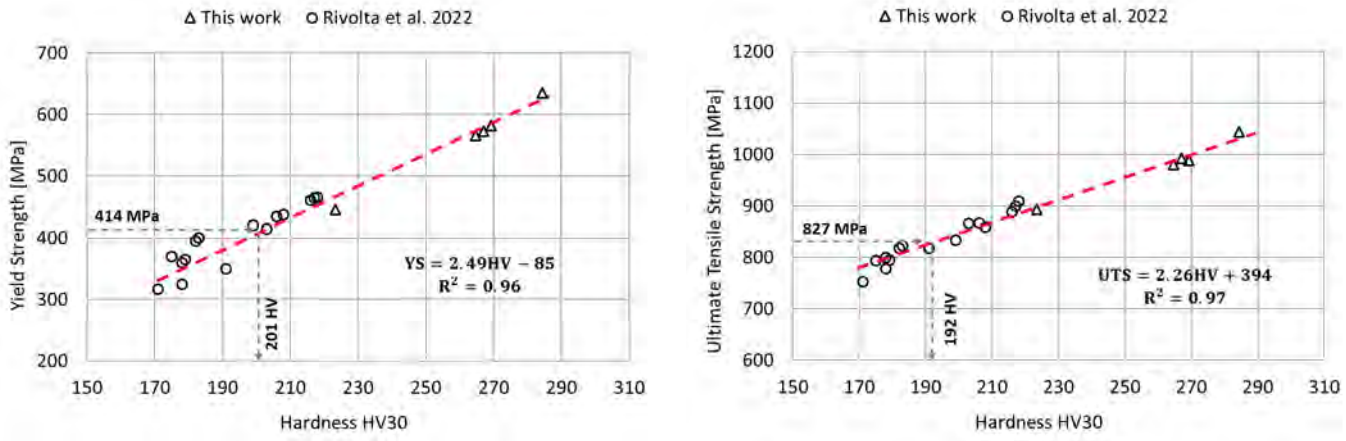

(**a**) (**b**)

Figure 10. Relationships between the tensile properties and the hardness via linear regression model. Data from the literature has been considered to improve the accuracy of the regression model [11]. (**a**) Relationship between the yield strength and the hardness; (**b**) Relationship between the ultimate tensile strength and the hardness.

The susceptibility to intergranular corrosion was investigated in a selection of the single- and double-aging conditions tested in this research. The corrosion rate limit was set equal to 1.20 mm/year, while the minimum hardness of 201 HV was determined based on the minimum standard requirement for the mechanical strength [12] and the hardness–yield strength relation defined in this paper. Therefore, a performance map was built and populated with the experimental conditions selected for the corrosion tests, as shown in Figure 11. The soft-annealed condition is acceptable only in terms of corrosion resistance. Upon single aging at 732 °C, the hardening effect is poor, and 16 h is required to exceed the minimum hardness requirement. However, at this exposure, the corrosion rate is significantly far from acceptability. At this temperature, such behavior is determined by the precipitation of intergranular chromium-rich carbides, which strongly reduce the corrosion resistance. On the other hand, upon single aging at 621 °C, the precipitation of γ'' precipitates is faster than the formation of intergranular carbides. In fact, at this temperature, as shown by the TTP diagram in Figure 1, the intergranular $M_{23}C_6$ carbides precipitate after aging times that are significantly longer than those required at 732 °C. Therefore, consistent with these observations, single aging at 621 °C for 72 h provides an acceptable combination of mechanical and corrosion properties, as shown in Figure 11. The formation of intergranular carbides was investigated in detail by SEM and EDXS analyses in selected conditions. As shown in Table 5, Figures 12 and 13, intergranular carbides were not detected upon single aging at 621 °C until 72 h. This observation justifies the presence of an acceptable corrosion resistance in this aging condition. Regarding single aging at 732 °C, discrete chains of intergranular carbides were identified in the sample aged for 16 h. No carbides were detected in the 1 h aged sample. As shown by the EDXS analyses reported in Table 5 and summarized in Figure 12, the chemical composition of the carbides observed in the 16 h aged sample (positions E, F and G of Figure 13f) was enriched in chromium and, to a lesser degree, in molybdenum, as also confirmed by the literature for $M_{23}C_6$ carbides [9,17]. The formation of these compounds agrees with the TTP curves available in the literature [9] and reported in Figure 1. Their occurrence is expected to decrease the corrosion resistance. As previously mentioned, at lower aging temperatures, such particles are absent, especially at 621 °C, where 72 h is not sufficient for the precipitation of such detrimental Cr-rich phases.

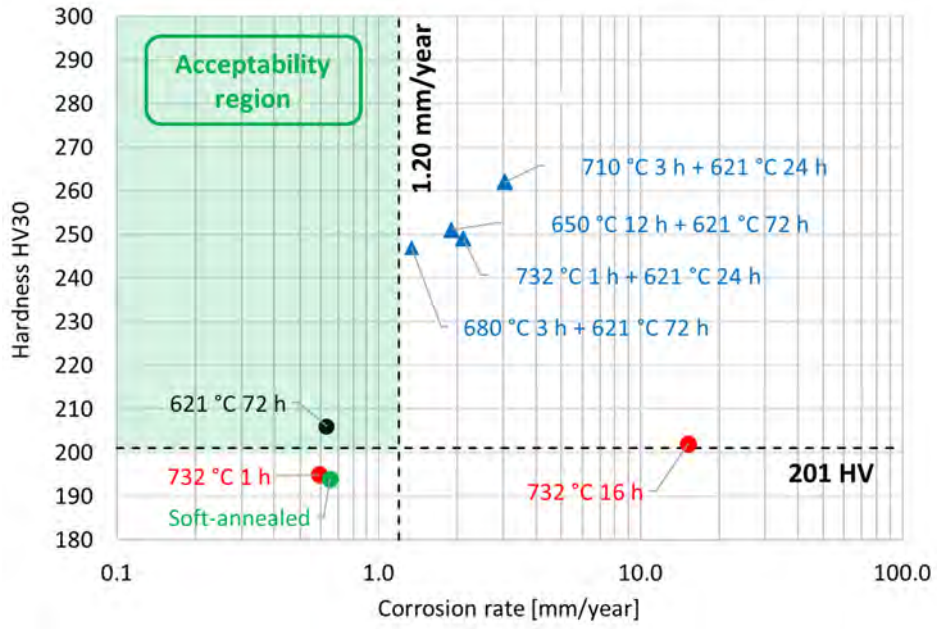

Figure 11. Performance map of the experimental conditions tested in this research work by hardness and corrosion tests. The two dashed lines represent the limit values for both the hardness and the corrosion rate according to the alloy performance requirements [12]. The acceptability region is highlighted by green shading.

Table 5. EDXS analyses in wt. % performed at the positions denoted on the SEM micrographs in Figure 13.

Figure	ID	Ni	Cr	Mo	Nb	Fe	Ti	Al	Si
Bulk (OES)	---	63.2	20.1	8.32	3.51	4.32	0.28	0.22	0.14
Figure 13b	A	62.1	21.5	8.21	3.20	4.41	0.26	0.16	0.16
Figure 13b	B	62.3	21.8	7.86	3.18	4.12	0.36	0.20	0.18
Figure 13d	C	61.9	22.0	7.78	2.96	4.53	0.31	0.37	0.15
Figure 13d	D	62.3	22.2	7.41	3.02	4.49	0.27	0.21	0.10
Figure 13f	E	55.1	27.7	8.61	4.15	3.74	0.34	0.15	0.21
Figure 13f	F	55.9	27.2	9.18	2.86	4.15	0.28	0.21	0.22
Figure 13f	G	56.5	26.7	8.22	3.55	4.34	0.31	0.19	0.19
Figure 13h	H	61.6	22.0	8.16	3.48	4.14	0.31	0.20	0.10
Figure 13h	I	61.7	22.2	7.95	3.21	4.37	0.27	0.18	0.17
Figure 13j	L	62.1	21.0	8.16	3.40	4.24	0.46	0.45	0.19
Figure 13j	M	62.0	21.6	8.21	3.38	4.08	0.31	0.24	0.18

Regarding the double-aging conditions tested by corrosion tests, we observed that the corrosion rate upon double aging does not confirm the behavior of the single-aging steps taken separately from each other. For instance, the condition of 732 °C for 1 h + 621 °C for 24 h is characterized by a corrosion rate of 2.1 mm/year. However, according to the experimental results, both 732 °C for 1 h and 621 °C for 24 h represent single-aging conditions acceptable in terms of corrosion resistance. The increase in the corrosion rate with their combination in the double-aging treatment was probably determined by the more pronounced formation of intermetallic γ'' precipitates, which also justifies the greater hardening effect. As reported in Figure 11, this behavior also affects the other double-aging conditions tested in this work.

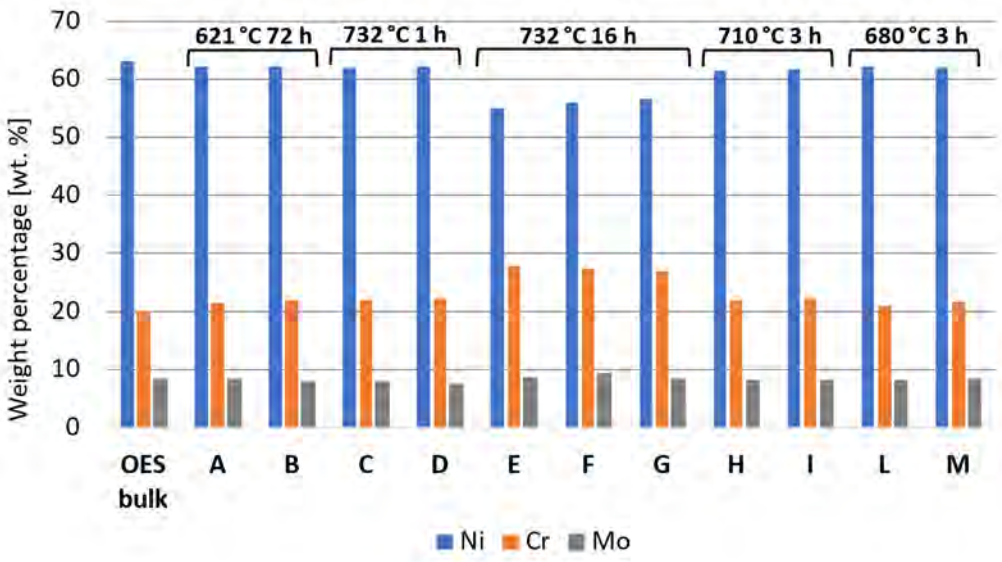

Figure 12. Nickel, chromium and molybdenum contents at the positions tested by EDXS analysis on the SEM micrographs shown in Figure 13 (values in wt. %). Summary of the data reported in Table 5.

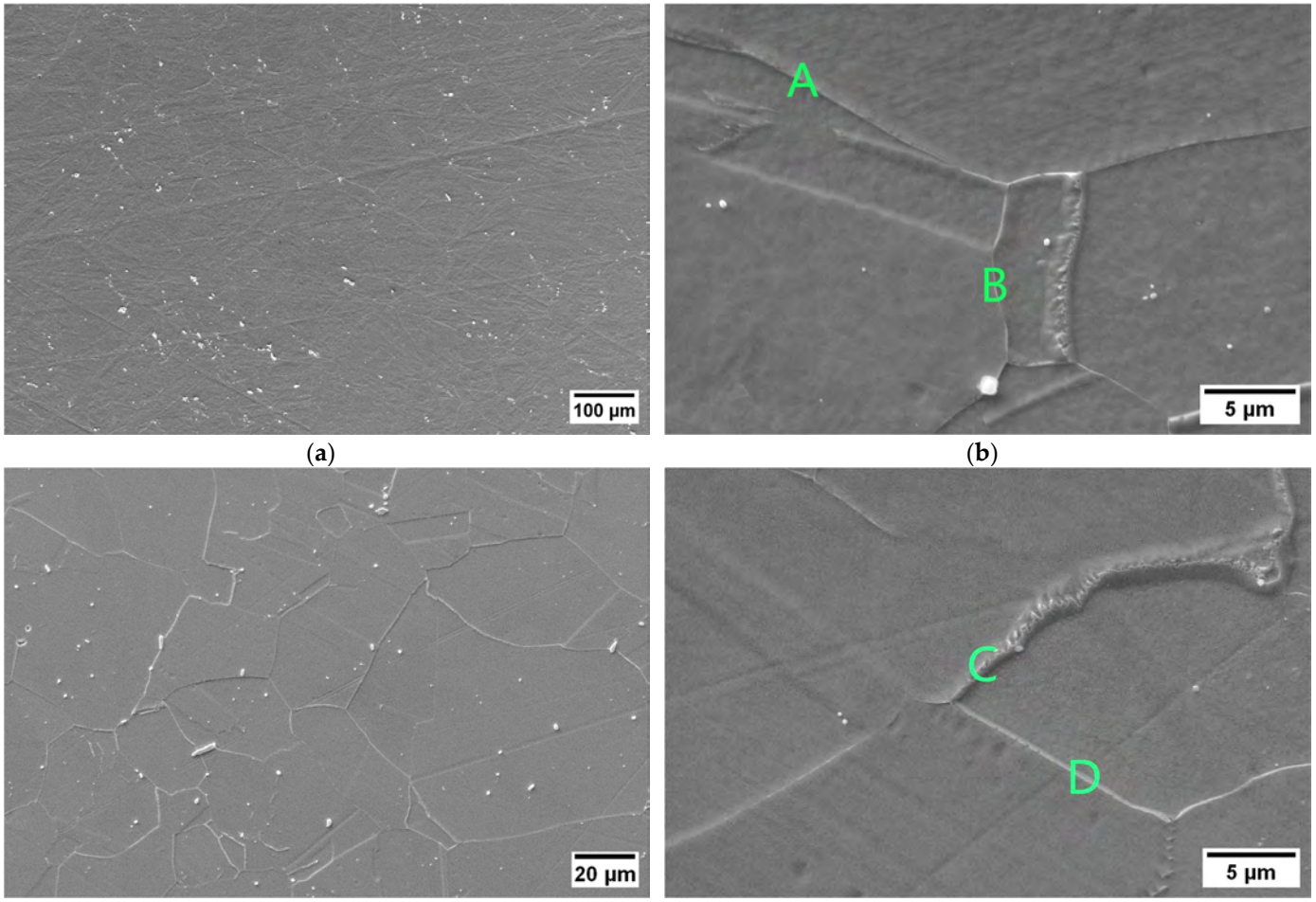

Figure 13. *Cont.*

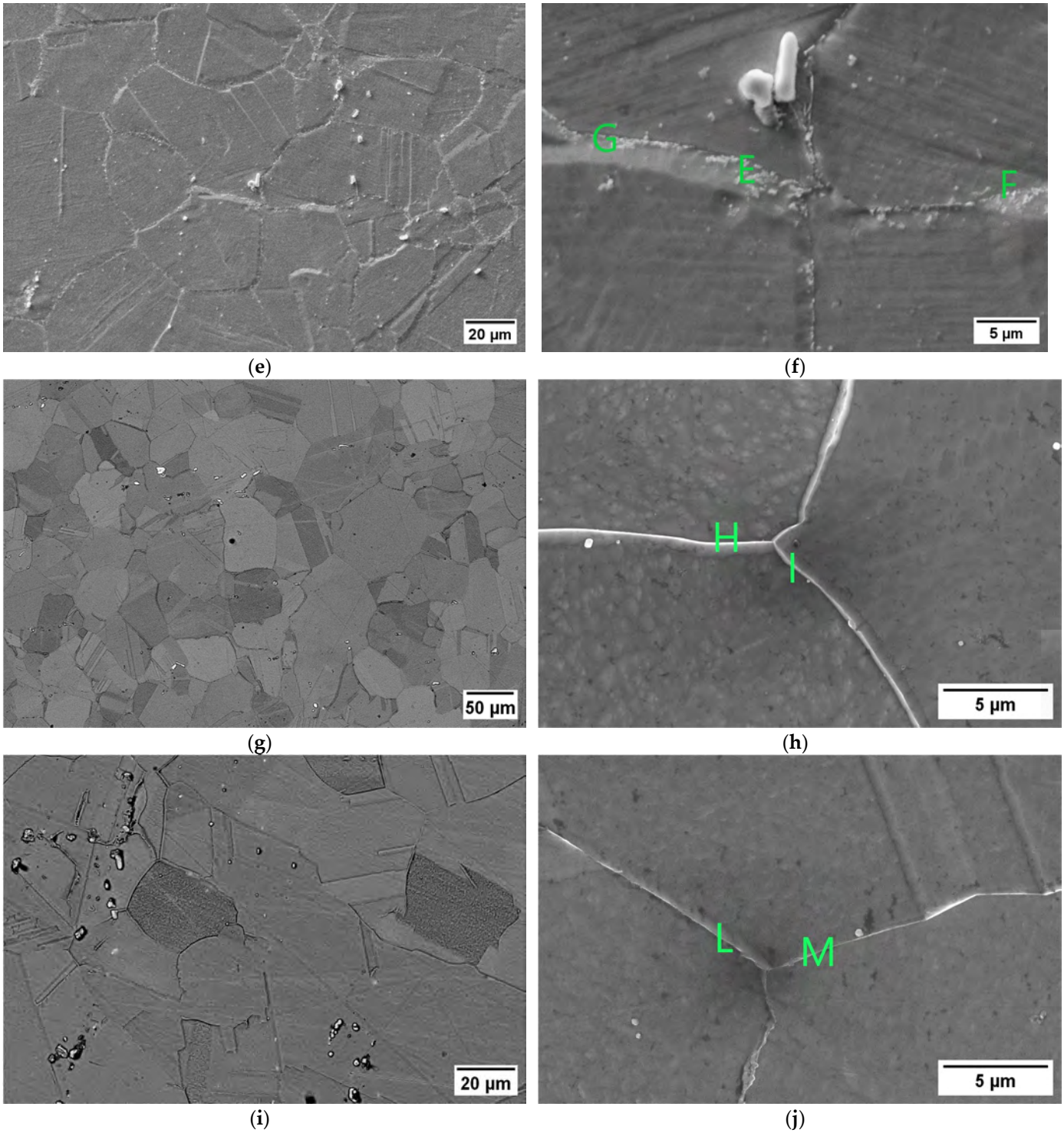

Figure 13. SEM micrographs of different single-aging conditions and positions of the EDXS analyses. (**a**,**b**) 621 °C 72 h; (**c**,**d**) 732 °C 1 h; (**e**,**f**) 732 °C 16 h; (**g**,**h**) 710 °C 3 h; (**i**,**j**) 680 °C 3 h. The letters represent the IDs of the EDXS analyses reported in Table 5 and summarized in Figure 12.

4. Conclusions

The mechanical and corrosion properties of Alloy 625 can be optimized using tailored aging treatments. This possibility can be exploited in the presence of an insufficient mechanical strength induced by excessive grain coarsening during processing and heat treatment.

- The soft-annealed material was associated with acceptable corrosion resistance but insufficient mechanical strength because of excessive grain growth;
- Excessively long aging exposures can activate the simultaneous formation of intermetallic phases and intergranular carbides. According to the SEM and EDXS observations, when chromium-rich carbides precipitated, sensitization was obtained. This negative effect was limited by the reduced aging temperature and time;
- With single aging at 732 °C, the hardening effect is poor, and 16 h is required to exceed the minimum hardness requirement. However, at this exposure, the corrosion rate is not acceptable;
- Only single aging at 621 °C for 72 h resulted in acceptable mechanical and corrosion properties. However, since the hardness is very close to the limit value estimated for acceptability, further investigation of longer aging times is necessary and will be considered in a future development of this work;
- The double-aging procedure allows γ'' precipitation to be accelerated due to the primary aging treatment, which promotes the nucleation and growth of subcritical γ'' nuclei. This triggering effect is necessary to reduce the overall heat treatment time, which would be significantly longer in the case of single aging at 621 °C without prior nucleation treatment. However, excessively long primary aging times do not provide any appreciable further acceleration of the age-hardening response;
- Primary aging is the most critical step for the resulting corrosion resistance. Even after optimization in terms of both temperature and time, none of the tested conditions were acceptable. A decrease in the primary aging temperature is useful for delaying the precipitation of intergranular carbides, but a weaker acceleration in the age-hardening response is obtained. An excessive reduction in the primary aging time is commonly not compatible with industrial applications involving large components;
- The Larson–Miller parameter was adopted in the regression model to combine the effects of the primary aging time and temperature. The double-aging process fraction curves for the hardness were modeled as a function of the Larson–Miller parameter for each tested secondary aging time, resulting in a good fit. This analysis revealed that for each curve, the steady-state hardness value was dependent on the secondary aging time.

Author Contributions: Conceptualization, B.R., R.G., D.P. and A.N.; methodology, R.G. and D.P.; formal analysis, R.G. and D.P.; investigation, B.R., R.G., D.P. and A.N.; writing—original draft preparation, D.P.; writing—review and editing, B.R., R.G., D.P. and A.N.; supervision, B.R. and R.G. All authors have read and agreed to the published version of the manuscript.

Funding: This research received no external funding.

Data Availability Statement: The raw data supporting the conclusions of this article will be made available by the authors on request.

Acknowledgments: The authors thank the technical staff (Agostino Silvestri) of the Laboratorio di Metallurgia e Prove Materiali—Sez. Meccanica "G. Silva" (Politecnico di Milano, Polo Territoriale di Lecco) for his valuable support regarding the experimental tests.

Conflicts of Interest: The authors declare no conflict of interest.

References

1. Suave, L.M.; Cormier, J.; Villechaise, P.; Soula, A.; Hervier, Z.; Bertheau, D.; Laigo, J. Microstructural Evolutions During Thermal Aging of Alloy 625: Impact of Temperature and Forming Process. *Metall. Mater. Trans. A* **2014**, *45*, 2963–2982. [CrossRef]
2. Shankar, V.; Rao, K.B.S.; Mannan, S.L. Microstructure and mechanical properties of Inconel 625 superalloy. *J. Nucl. Mater.* **2001**, *288*, 222–232. [CrossRef]
3. Sukumaran, A.; Gupta, R.K.; Kumar, V.A. Effect of Heat Treatment Parameters on the Microstructure and Properties of Inconel-625 Superalloy. *J. Mater. Eng. Perform.* **2017**, *26*, 3048–3057. [CrossRef]
4. Heubner, U.; Kloewer, J.; Alves, H.; Behrens, R.; Schindler, C.; Wahl, V.; Wolf, M. *Nickel Alloys and High-Alloyed Special Stainless Steels: Properties-Manufacturing-Applications*, 4th ed.; Expert-Verlag: Renningen, Germany, 2012.
5. ASM International. *ASM Specialty Handbook: Nickel, Cobalt, and Their Alloys*; ASM International: Materials Park, OH, USA, 2000.

6. Donachie, M.J.; Donachie, S.J. *Superalloys: A Technical Guide*, 2nd ed.; ASM International: Materials Park, OH, USA, 2002.
7. Eiselstein, H.L.; Tillack, D.J. The Invention and Definition of Alloy 625. In *Proceedings on Superalloys 718, 625, and Derivatives*; Loria, E.A., Ed.; The Minerals, Metals & Materials Society: Pittsburgh, PA, USA, 1991; pp. 1–14.
8. Durand-Charre, M. *The Microstructure of Superalloys*, 1st ed.; Routledge: London, UK, 1968.
9. Floreen, S.; Fuchs, G.E.; Yang, W.J. The Metallurgy of Alloy 625. In *Superalloys 718, 625, 706 and Derivatives*; The Minerals, Metals & Materials Society: Pittsburgh, PA, USA, 1994; pp. 13–37.
10. Patel, S.J.; Smith, G.D. The Role of Niobium in Wrought Precipitation-Hardened Nickel-Base Alloys. In *Proceedings on Superalloys 718, 625, 706 and Derivatives*; Loria, E.A., Ed.; The Minerals, Metals & Materials Society: Pittsburgh, PA, USA, 2005; pp. 135–154.
11. Rivolta, B.; Boniardi, M.V.; Gerosa, R.; Casaroli, A.; Panzeri, D.; Zordão, L.H.P. Alloy 625 Forgings: Thermo-Metallurgical Model of Solution-Annealing Treatment. *J. Mater. Eng. Perform.* **2022**, *32*, 5785–5797. [CrossRef]
12. *ASTM B446-19*; Standard Specification for Nickel-Chromium-Molybdenum-Columbium Alloy (UNS N06625), Nickel-Chromium-Molybdenum-Silicon Alloy (UNS N06219), and Nickel-Chromium-Molybdenum-Tungsten Alloy (UNS N06650) Rod and Bar. ASTM International: Materials Park, OH, USA, 2019.
13. VMD Metals International GmbH, VDM Alloy 625 Nicrofer 6020 hMo. 2018. Available online: https://www.vdm-metals.com/en/alloy625/ (accessed on 1 May 2020).
14. Reed, R.C.; Rae, C.M.F. Physical Metallurgy of the Nickel-Based Superalloys. In *Physical Metallurgy*; Elsevier: Amsterdam, The Netherlands, 2014; pp. 2215–2290. [CrossRef]
15. Liu, X.; Fan, J.; Zhang, P.; Cao, K.; Wang, Z.; Chen, F.; Liu, D.; Tang, B.; Kou, H.; Li, J. Influence of heat treatment on Inconel 625 superalloy sheet: Carbides, γ'', δ phase precipitation and tensile deformation behavior. *J. Alloys Compd.* **2023**, *930*, 167522. [CrossRef]
16. Yenusah, C.O.; Ji, Y.; Liu, Y.; Stone, T.W.; Horstemeyer, M.F.; Chen, L.-Q.; Chen, L. Three-dimensional Phase-field simulation of γ'' precipitation kinetics in Inconel 625 during heat treatment. *Comput. Mater. Sci.* **2021**, *187*, 110123. [CrossRef]
17. Yu, L.-J.; Marquis, E.A. Precipitation behavior of Alloy 625 and Alloy 625 plus. *J. Alloys Compd.* **2019**, *811*, 151916. [CrossRef]
18. Sundararaman, M.; Kumar, L.; Prasad, G.E.; Mukhopadhyay, P.; Banerjee, S. Precipitation of an intermetallic phase with Pt2Mo-type structure in alloy 625. *Metall. Mater. Trans. A* **1999**, *30*, 41–52. [CrossRef]
19. Suave, L.M.; Bertheau, D.; Cormier, J.; Villechaise, P.; Soula, A.; Hervier, Z.; Laigo, J. Impact of microstructural evolutions during thermal aging of Alloy 625 on its monotonic mechanical properties. *MATEC Web Conf.* **2014**, *14*, 21001. [CrossRef]
20. Vernot-Loier, C.; Cortial, F. Influence of Heat Treatments on Microstructure, Mechanical Properties and Corrosion Behaviour of Alloy 625 Forged Rod. In *Proceedings on Superalloys 718, 625, and Derivatives*; Loria, E.A., Ed.; The Minerals, Metals & Materials Society: Pittsburgh, PA, USA, 1991; pp. 409–422.
21. Heubner, U.; Köhler, M. Effect of Carbon Content and Other Variables on Yield Strength, Ductility, and Creep Properties of Alloy 625. In *Proceedings on Superalloys 718, 625, 706 and Derivatives*; Loria, E.A., Ed.; The Minerals, Metals & Materials Society: Pittsburgh, PA, USA, 1994; pp. 479–488.
22. Heubner, U.; Köhler, M. The effect of final heat treatment and chemical composition on sensitization, strength and thermal stability of alloy 625. In *Proceedings on Superalloys 718, 625, 706 and Derivatives*; The Minerals, Metals & Materials Society: Pittsburgh, PA, USA, 1997; pp. 795–803.
23. Liu, M.; Zheng, W.; Xiang, J.; Song, Z.; Pu, E.; Feng, H. Grain Growth Behavior of Inconel 625 Superalloy. *J. Iron Steel Res. Int.* **2016**, *23*, 1111–1118. [CrossRef]
24. Moore, I.J.; Taylor, J.I.; Tracy, M.W.; Burke, M.G.; Palmiere, E.J. Grain coarsening behaviour of solution annealed Alloy 625 between 600–800 °C. *Mater. Sci. Eng. A* **2017**, *682*, 402–409. [CrossRef]
25. Guo, S.; Li, D.; Guo, Q.; Wu, Z.; Peng, H.; Hu, J. Investigation on hot workability characteristics of Inconel 625 superalloy using processing maps. *J. Mater. Sci.* **2012**, *47*, 5867–5878. [CrossRef]
26. Chen, X.; Nie, L.-Y.; Hu, H.; Lin, Y.C.; Liu, Y.-X.; Wu, Z.-L.; Zhou, X.; Zhang, J.; Lu, X. High-temperature deformation characteristics and constitutive models of Inconel 625 superalloy. *Mater. Today Commun.* **2022**, *32*, 103855. [CrossRef]
27. Jia, Z.; Gao, Z.; Ji, J.; Liu, D.; Guo, T.; Ding, Y. Study of the Dynamic Recrystallization Process of the Inconel 625 Alloy at a High Strain Rate. *Materials* **2019**, *12*, 510. [CrossRef] [PubMed]
28. Carpenter Technology Corporation. *CarTech®Custom Age 625 PLUS®Alloy: Technical Datasheet*; Carpenter Technology Corporation: Pennvania, PA, USA, 2020; Available online: www.carpentertechnology.com/alloy-finder/625-Plus (accessed on 25 August 2020).
29. Schmidt, N.B.; DeBold, T.A.; Frank, R.B. Custom age 625®plus alloy—A higher strength alternative to alloy 625. *J. Mater. Eng. Perform.* **1992**, *1*, 483–488. [CrossRef]
30. *ASTM G28-02*; Standard Test Methods for Detecting Susceptibility to Intergranular Corrosion in Wrought, Nickel-Rich, Chromium-Bearing Alloys. ASTM International: Materials Park, OH, USA, 2015.
31. *E407-07*; Standard Practice for Microetching Metals and Alloys. ASTM International: Materials Park, OH, USA, 2015.
32. Carpenter Technology Corporation. *A Guide to Etching Specialty Alloys for Microstructural Evaluation*; Carpenter Technology Corporation: Pennvania, PA, USA, 2020; Available online: https://carpentertechnology.com/blog/a-guide-to-etching-specialty-alloys (accessed on 14 November 2023).
33. *ASTM E112-13*; Standard Test Methods for Determining Average Grain Size. ASTM International: Materials Park, OH, USA, 2013. [CrossRef]

34. *ISO 6507-1:2018*; Metallic Materials–Vickers Hardness Test. BSI Standards Publication: London, UK, 2018.
35. *BS EN ISO 6892-1:2019*; Metallic materials-Tensile Testing. BSI Standards Publication: London, UK, 2020.